Eur Radiol (2016) 26:3301–3309
DOI 10.1007/s00330-015-4152-y

CONTRAST MEDIA

Development of silica-encapsulated silver nanoparticles as contrast agents intended for dual-energy mammography

Roshan Karunamuni[1] · Pratap C. Naha[2] · Kristen C. Lau[1] · Ajlan Al-Zaki[1] · Anatoliy V. Popov[2] · Edward J. Delikatny[2] · Andrew Tsourkas[1] · David P. Cormode[2] · Andrew D. A. Maidment[2]

Received: 19 March 2015 / Revised: 13 November 2015 / Accepted: 30 November 2015 / Published online: 24 February 2016

Abstract
Objective Dual-energy (DE) mammography has recently entered the clinic. Previous theoretical and phantom studies demonstrated that silver provides greater contrast than iodine for this technique. Our objective was to characterize and evaluate in vivo a prototype silver contrast agent ultimately intended for DE mammography.
Methods The prototype silver contrast agent was synthesized using a three-step process: synthesis of a silver core, silica encapsulation and PEG coating. The nanoparticles were then injected into mice to determine their accumulation in various organs, blood half-life and dual-energy contrast. All animal procedures were approved by the institutional animal care and use committee.
Results The final diameter of the nanoparticles was measured to be 102 (±9) nm. The particles were removed from the vascular circulation with a half-life of 15 min, and accumulated in macrophage-rich organs such as the liver, spleen and lymph nodes. Dual-energy subtraction techniques increased the signal difference-to-noise ratio of the particles by as much as a factor of 15.2 compared to the single-energy images. These nanoparticles produced no adverse effects in mice.
Conclusion Silver nanoparticles are an effective contrast agent for dual-energy x-ray imaging. With further design improvements, silver nanoparticles may prove valuable in breast cancer screening and diagnosis.

✉ Andrew D. A. Maidment
andrew.maidment@uphs.upenn.edu

[1] Department of Bioengineering, University of Pennsylvania, Philadelphia, PA, USA

[2] Department of Radiology, University of Pennsylvania, 1 Silverstein, 3400 Spruce Street, Philadelphia, PA 19104, USA

Key Points
- *Silver has potential as a contrast agent for DE mammography.*
- *Silica-coated silver nanoparticles are biocompatible and suited for in vivo use.*
- *Silver nanoparticles produce strong contrast in vivo using DE mammography imaging systems.*

Keywords Dual-energy · Mammography · Nanoparticles · Silver · Gold · Breast cancer

Introduction

Mammography is widely used to screen for breast cancer. Despite the effectiveness of mammography screening, improvements to sensitivity could be made, especially for women with dense breasts [1]. Therefore, alternative methods for breast cancer screening are being developed. For example, contrast-enhanced (CE) breast imaging, such as CE magnetic resonance imaging (MRI) and dual-energy (DE) mammography, has been used to detect and quantify blood flow changes associated with tumorigenic neovasculature to improve overall cancer detection [2–6]. DE mammography provides high spatial resolution images similar to those of digital mammography, together with perfusion data, in a single, inexpensive and quick imaging procedure [2].

In DE mammography, two images [low energy (LE) and high energy (HE)] of the breast are acquired at different tube voltages, e.g. 26 and 49 kV [7]. These voltages are selected to place the two spectra on either side of the photoelectric K-absorption edge of a vascular imaging agent. By applying a pixel-by-pixel weighted subtraction of the two images, the signal arising from the contrast agent can be separated from

that of the surrounding background structure to yield an image consisting primarily of vascular information.

Currently, DE imaging is performed with iodinated contrast agents. However, these agents have several deficiencies. The high K-edge energy of iodine (33.2 keV) is not well suited for the lower energies (26 to 49 kV) used in DE mammography. Furthermore, iodinated agents produce allergic reactions in some patients and can cause contrast-mediated nephropathy at high doses [8, 9]. While metal nanoparticles based on gold, bismuth or ytterbium have recently been reported for multi-energy computed tomography imaging techniques [10–13], agents specifically designed for DE mammography are yet to be reported.

Silver (Ag) has been identified as a new candidate agent for DE mammography that can provide more contrast than iodine at clinically utilized imaging protocols [14–16]. The lower K-edge energy of silver (25.5 keV) provides two key benefits. First, the optimal LE imaging technique is a classically used technique for soft-tissue anatomic imaging clinically. Second, there is greater flexibility in the choice of the HE spectrum, allowing for optimal selection. Analytic modelling together with experimental validation in phantoms [14, 16] demonstrates that if the established technique parameters currently utilized in the clinic are considered, silver provides higher values of signal difference-to-noise ratio (SDNR) than iodine. In particular, the SDNR of silver was found to be 43 % higher than that of iodine when using the optimal DE imaging parameters for each contrast agent [15]. This suggests that silver is better suited as a contrast agent in the mammographic energy range. A biologically stable silver agent could therefore be translated to the clinic without the need for modification of protocol or imaging system.

Nano-silver represents the largest (25 %) and fastest growing category of nanotechnology-based consumer products [17]. A nanoparticle-based agent might be the best type of formulation as nanoparticles tend to accumulate in tumours as a result of the enhanced permeability and retention effect, which would result in greater contrast in the tumours [18]. To our knowledge, there has been no prior report on the development of silver nanoparticles as DE contrast agents. In this work, we report a novel silver nanoparticle-based agent, specifically designed for DE mammography (Fig. 1). We herein describe the synthesis, characterization and in vivo imaging in mice of this prototype silver-based contrast agent.

Materials and methods

Materials

Polyvinylpyrrolidone (average molecular weight 10,000 Da), silver nitrate, ammonium hydroxide, tetraethoxysilane and 3-aminopropyltrimethoxysilane were purchased from Sigma-Aldrich (St Louis, MO). Polyethylene glycol-*N*-succinimidyl ester was purchased from Creative PEG Works (Winston Salem, NC). All other chemicals were purchased from Fisher Scientific (Waltham, MA). Female mice (6–8 weeks) were purchased from Charles River Laboratory (Wilmington, MA). All animal studies were approved by the Institutional Animal Care and Use Committee at the University of Pennsylvania.

Synthesis of silver core

Silver cores were synthesized as described by Silvert et al. [19]. Thus 1.5 g of polyvinylpyrrolidone (PVP) was dissolved in 75 mL of ethylene glycol overnight and 50 mg of silver nitrate ($AgNO_3$) was then added. The mixture was heated to 120 °C at a rate of 1 °C/min. The reaction was allowed to proceed at this temperature for 1 h. The mixture was then cooled to room temperature. The PVP-stabilized silver nanoparticles were purified by adding acetone to the reaction vessel and centrifuging at 4000×*g* for 15 min. The particles were then resuspended in ethyl alcohol for further modification.

The PVP-stabilized silver cores were encapsulated within a silica (SiO_2) shell using the method described by Graf et al. [20]. Thus 415 μL of ammonium hydroxide was added to 9.438 mL of PVP-stabilized silver nanoparticles, after which 75 μL of tetraethoxysilane (TEOS) in 675 μL of ethyl alcohol was added. The reaction was then allowed to proceed in the dark for 12 h. The silica–silver nanoparticles were purified by centrifugation at 19,000×*g* for 15 min, and resuspended in ethyl alcohol. The silica-encapsulated nanoparticles were reacted with 3-aminopropyltrimethoxysilane under gentle stirring for 12 h at room temperature, after which the temperature of the reaction was brought up to 55 °C for 1 h.

PEG stabilization of silica–silver nanoparticles

The amine-terminated silica–silver nanoparticles were resuspended in 10 mL of phosphate buffered saline (PBS). The particles were mixed with 100 mg of PEG-*N*-succinimidyl ester (PEG molecular weight 3400 Da) and allowed to react for 2 h under vigorous stirring at room temperature. The PEG-coated silica–silver nanoparticles (PEG-SiO_2Ag) were then purified using a combination of Amicon Ultra-15 centrifugal filter units (EMD Millipore, Billerica, MA, USA) and 0.2-μm surfactant-free cellulose acetate (SFCA) syringe filters to remove any unwanted by-products and excess reagents.

Gold nanoparticle synthesis

PEG-coated gold nanoparticles were used as a control for in vivo imaging experiments. The synthesis was performed as previously described [21–23]. In short, 50 mg of gold

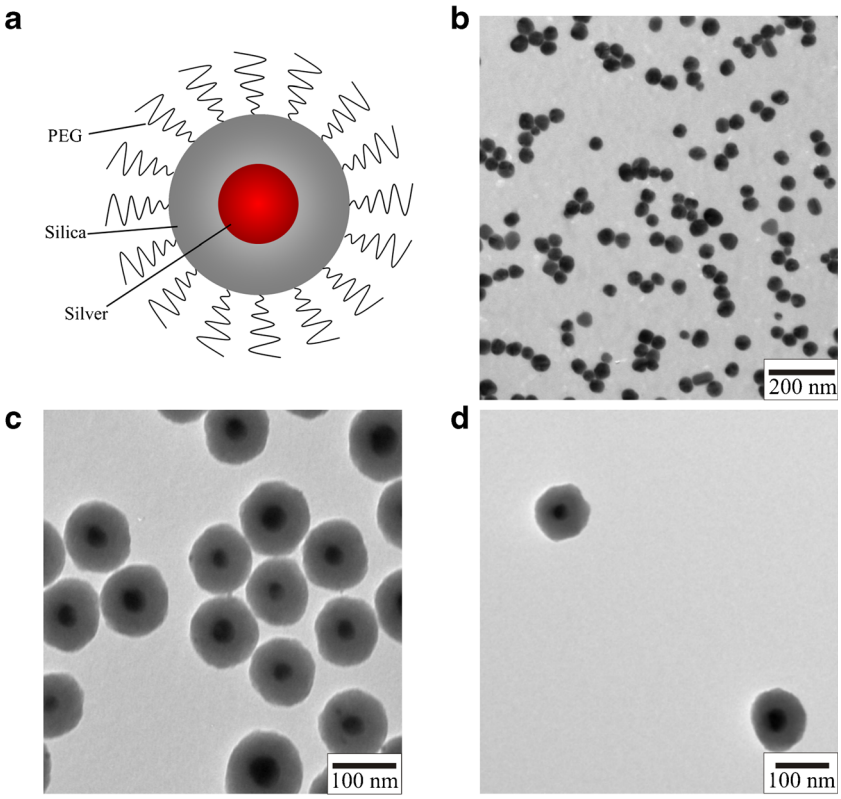

Fig. 1 **a** Design of prototype silver nanoparticle imaging agent. TEM micrographs of **b** polyvinylpyrrolidone-coated silver cores, **c** silica-encapsulated silver cores and **d** polyethylene glycol–silica–silver nanoparticles (PEG-SiO_2Ag)

chloride was dissolved in 500 mL of deionized water and brought to a boil. Then 17.5 mL of 1 % sodium citrate was added, whereupon the colour of the solution changed from a pale yellow to a deep red. The solution was stirred vigorously for 30 min after which it was allowed to cool to room temperature. Then 100 mg of thiol-terminated methoxy PEG-2000 dissolved in 50 mL of deionized water was added and the solution was stirred gently at room temperature for 16 h. The solution was then washed three times with PBS and concentrated using molecular weight cut-off concentrator tubes (10,000 Da). The solution was sterilized using syringe filtration (0.2 μm). The cores were spherical and 15 nm in diameter, while the hydrodynamic diameter was 21 nm.

Nanoparticle characterization

The physical diameter of the nanoparticles was measured using a JEOL 1010 (JEOL, Peabody, MA, USA) transmission electron microscope. The diameters of 100 particles were measured, and the average diameter of this sample was calculated. The hydrodynamic diameter of the nanoparticles was measured using a Malvern Instruments Zetasizer (Malvern Instruments, Malvern, UK). The silver concentration was determined using inductively coupled plasma optical emission spectroscopy (ICP–OES) with a Spectro Genesis (Spectro, Kleve, Germany).

Pharmacokinetic/biodistribution study

PEG-SiO_2Ag was injected via a tail vein into three female mice between 8 and 10 weeks old at a dose of 400 mg/kg. Then 10-μL samples of blood were obtained pre-injection and at various time points post-injection (5 min, 10 min, 15 min, 30 min, 1 h, 2 h, 4 h, 8 h, 24 h). The animals were sacrificed 24 h after injection of the particles. The organs of the animals were harvested and digested, along with the blood samples, using 1 M nitric acid at room temperature for 1 h. The silver content was then measured using the aforementioned ICP–OES system.

DE imaging of mice

The silver contrast agent was administered at a dose of 400 mg/kg of silver via subcutaneous, intraperitoneal and intravenous injections into three female mice for each injection route. These routes were used to ensure a high concentration of agent in focal locations and to allow distinct images to be acquired. Controls were mice injected with either saline or gold nanoparticles (also 400 mg/kg). The mice were maintained under anaesthesia for the entirety of the imaging procedure using 2 % inhaled isoflurane. The animals were imaged using a GE Senographe DS mammography unit (GE Healthcare, Little Chalfont, UK) and a Hologic Selenia Dimensions DE prototype (Hologic, Bedford, MA). For the

GE unit, the HE and LE spectra were selected as 49 kV rhodium target with rhodium filtration and a 26 kV molybdenum target with molybdenum filtration, respectively. For the Hologic prototype, the HE and LE spectra were selected as 45 kV tungsten target with copper filtration and a 26 kV tungsten target with silver filtration, respectively. In both cases, the LE kV was set just below the K-edge of Ag, while the HE kV was set to minimize overlap between the two spectra.

Regions of interest were chosen in the soft tissue (s) and bone (b) in the LE and HE images. A weighting factor (W) was applied to the LE image in order to remove the background structures (bone, soft tissue) in the DE image. W was calculated to be analogous to previous formulations [14], using the average signal intensities (SI) of the bone and soft tissue regions:

$$W = \frac{\ln\left(\mathrm{SI}_{\mathrm{b}}^{\mathrm{HE}}\right) - \ln\left(\mathrm{SI}_{\mathrm{s}}^{\mathrm{HE}}\right)}{\ln\left(\mathrm{SI}_{\mathrm{b}}^{\mathrm{LE}}\right) - \ln\left(\mathrm{SI}_{\mathrm{s}}^{\mathrm{LE}}\right)}.$$

The DE image was calculated as the weighted logarithmic subtraction between the LE and HE image.

$$\mathrm{DE} = \ln(\mathrm{HE}) - W\ln(\mathrm{LE})$$

Prior to DE subtraction, the HE image was registered to the LE image using the Advanced Normalization Tools software package (Penn Image Computing & Science Lab, Philadelphia, PA) to correct for motion occurring between image acquisitions [24]. An intensity-based image registration algorithm was used. Large-scale motions were first corrected using a mutual information optimization and affine transformation. A normalized cross-correlation (CC) metric was then used with a diffeomorphic transform to correct for misalignment at finer scales. This iterative hybrid registration approach is based on the multi-scale, deformable registration method for dual-energy x-ray images developed by Gang et al. [25]. For the purpose of display, all images were denoised by application of a 3×3 median filter, and the LE and HE images were unsharp masked to enhance anatomic details.

Results

Characterization of nanoparticles

The physical diameter of the silver nanoparticles at various stages of the synthesis was measured using transmission electron microscopy (TEM). The PVP-coated silver cores are shown in Fig. 1b. The particles consist of solid, spherical silver cores with an average diameter of 39 ± 6 nm (mean ± standard deviation). A silica coating was applied to provide an inert particle for testing and a surface upon which robust PEGylation is possible. After silica encapsulation, the total diameter of the nanoparticles was 102 ± 9 nm (Fig. 1c). The majority of the silica–silver nanoparticles consisted of a single silver core covered by a spherical silica shell. The PEG layer of the final PEG-SiO_2Ag is electron-transparent and thus does not appear in the TEM micrograph (Fig. 1d). The hydrodynamic diameter and zeta potential of PEG-SiAg was determined to be 115.3 nm (polydispersity index of 10 %) and 0.1 mV, respectively. The difference of 13.2 nm between the physical and hydrodynamic diameters indicates that the PEG ligands cover some of the SiO_2 surface.

Blood clearance/biodistribution

The blood clearance and biodistribution results are shown in Fig. 2a and b, respectively. These aspects were investigated via intravenous injection, since this would be the clinical route of administration. The particles are rapidly removed from the bloodstream with a half-life of 15 min, with only trace amounts of silver nanoparticles circulating 24 h after injection. The particles are taken up by the liver, spleen and lymph nodes. Significant accumulation of silver was also detected in the pancreas, large bowel and muscle.

DE imaging of mice: subcutaneous administration

We performed imaging experiments using subcutaneous, intraperitoneal and intravenous injections. LE, HE and DE images of a mouse after subcutaneous injection of the silver contrast agent are shown in Fig. 3a–c, where the site of injection is indicated with a long arrow. As can be seen, the single-energy images (LE and HE) show good contrast between the various tissue types, allowing for straightforward discrimination between bone and soft tissue. The anatomical contrast is substantially decreased in the DE image, while the contrast agent is markedly more conspicuous in the DE image than the HE or LE image. The silver contrast agent is strongly conspicuous in the DE image because of the differential contrast between the LE and HE images; the silver produces more contrast in the HE image than in the LE image, which is acquired below the K-edge of silver.

For comparison, images of a mouse with a saline injection, as well as a mouse injected with gold nanoparticles are also shown in Fig. 3d–f and g–i respectively. In both cases, little to no contrast is observed after the anatomical signal variation has been removed using DE-weighted subtraction. This occurs because neither saline nor gold has a K-edge in the energy range of 26–49 kV. As a result, both saline and gold are subtracted with the tissue in the DE image. There is a small residual signal for the Au nanoparticles in the DE image (Fig. 3i); however, this signal is much smaller than in the LE or HE images; we attribute this residual signal to detector nonlinearity.

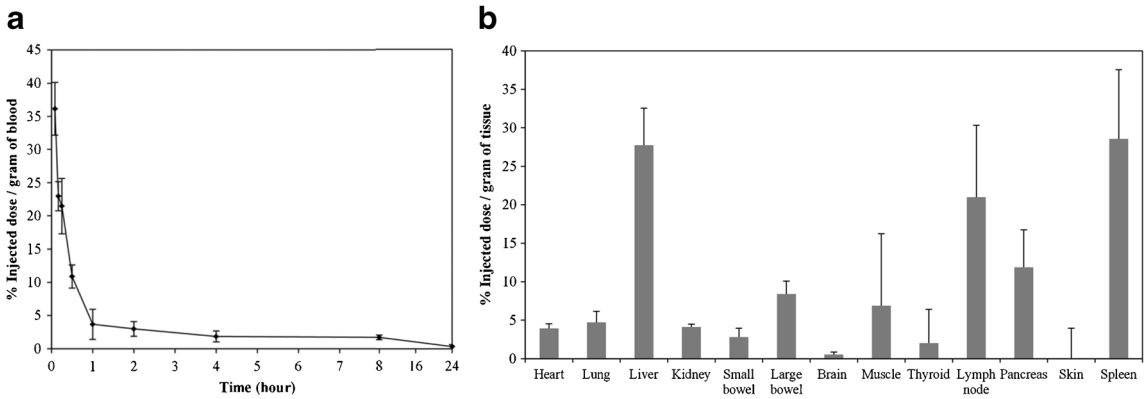

Fig. 2 **a** Blood clearance of PEG-SiO_2Ag nanoparticles after intravenous injection into three female mice. The plasma half-life of the nanoparticles was calculated to be 15 min. *Error bars* represent standard deviations. **b** Biodistribution of PEG-SiO_2Ag nanoparticles, 24 h after intravenous injection into female mice. The majority of the particles are located in the liver and spleen, in addition to accumulation in the lymph nodes, large bowel and muscle. The remaining organs showed very little uptake of the silver particles. *Error bars* represent standard deviation

The residual non-silver contrast in the DE images of the mice can be attributed to three sources. First, DE subtraction is sensitive to the total thickness of tissue in the beam path. This is remedied in clinical DE breast imaging by applying compression to the breast to allow for a homogenous thickness of imaged tissue, and by image post-processing. This was not performed in the mouse experiments, and therefore the residual signal varies with thickness; this is most evident in the extremities of the animal. This is also evident in gas-filled cavities including the large intestines and the lungs (wide arrows). Second, the subtraction method is designed to cancel the signals from soft tissue and bone. Materials with markedly different composition from the tissues of the mouse can be present. Minerals included in the mouse's food and contamination in the fur (hollow arrows) are visible even after subtraction. Finally, regions of high or low intensity (white/black) at the diaphragm are the result of registration errors between the LE and HE images arising from differences in respiration during image acquisition. The outlines of some bones in the DE images are similarly the result of subpixel shifts that cannot be corrected by registration.

The silver contrast agent can be identified in all three images in Fig. 3a–c. However, the DE image is able to discriminate between the injected nanoparticles and the underlying bony anatomical structures. The boundaries of the injection site can be easily identified and separated from the surrounding tissue structures. The signal difference-to-noise ratio (SDNR) of the silver contrast agent (Ag) compared to the background bone or soft (B) tissue was calculated as:

$$\mathrm{SDNR} = \frac{\mathrm{SI}^{\mathrm{Ag}} - \mathrm{SI}^{\mathrm{B}}}{\sigma^{\mathrm{B}}},$$

where SI is the average signal intensity and σ is the standard deviation of a region of interest chosen in either the silver contrast agent or bone. The SDNR versus bone was calculated as 1.5, 0.7 and 10.6 in the LE, HE and DE images respectively, indicating a 7.1 to 15.2 factor improvement in the contrast of the silver in the DE image compared to the single-energy images. The SDNR versus soft tissue was calculated as 1.8, 2.6 and 9.0, a 3.5- to 5.0-fold improvement compared to the single-energy images. The increase in the SDNR compared to bone is due to the greatly reduced bone signal in the DE image.

DE imaging of mice: intraperitoneal administration

LE, HE and DE images of an animal after intraperitoneal injection are shown in Fig. 4. The suppression of the anatomical signal in the DE image highlights the abdominal organs after the surrounding space has been filled with the silver contrast agent. The progression of the contrast in the peritoneal cavity over time is illustrated by comparing the two time points. At 5 min post-injection, the contrast agent is still broadly distributed through the abdomen. This is seen from the overall increase in contrast in the abdomen (Fig. 4c, long arrows), and also the outline of specific organs, such as the bladder (Fig. 4c, short arrows). By 40 min post-injection, small focal aggregations of contrast agent are observed in the peritoneal cavity. The advantages of DE imaging are clearly shown, because the DE image visualizes the contrast agent regardless of whether soft tissues (Fig. 4f, short arrow) or vertebrae (Fig. 4f, long arrow) overlap. This is different from the HE image, which visualizes the contrast agent in soft tissues (Fig. 4e, short arrow), but obscures the contrast agent with the vertebrae (Fig. 4e, long arrow).

DE imaging of mice: intravenous administration

LE, HE and DE images of an animal after intravenous injection are shown in Fig. 5. The image was acquired 8 min post-injection. As with the other routes of injection, the viscera and skeleton seen in the LE and HE images are suppressed in the

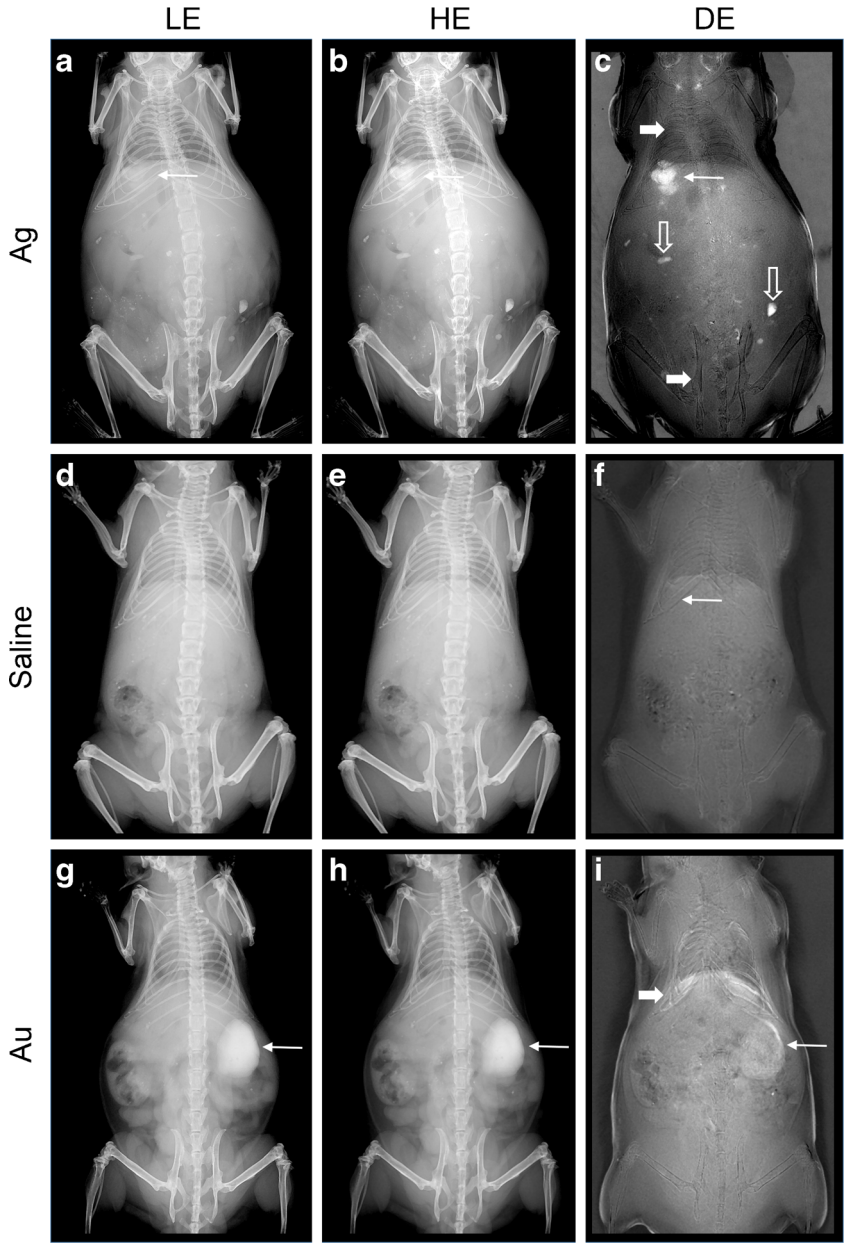

Fig. 3 LE, HE and DE images of mice immediately after administration via subcutaneous injection of the silver contrast agent (**a**–**c**), saline (**d**–**f**) and gold nanoparticles (**g**–**i**). DE subtraction emphasizes the signal of the silver contrast agent

DE image. Some residual signal is seen for gas-filled cavities, and where the bony structures overlap, such as where the thoracic vertebrae and posterior ribs are superimposed. The DE image clearly shows the heart (Fig. 5c, long arrow) and the abdominal aorta (short arrows). Smaller vessels, including the celiac artery and associated branches, and the upper femoral arteries are also visualized to some degree. Note that in this lateral projection, the ribs and sternum, which overlap the heart, do not affect the visualization of the silver contrast agent.

In all cases, the animals were still alive and exhibiting no signs of distress up to 2 months after the injection of the particles, at which point they were euthanized.

Discussion

Silver has been proposed as a potential alternative to iodine for use as a DE contrast agent. Little or no modifications to the imaging system or protocol are needed to obtain a higher contrast with silver, implying that a viable silver contrast agent could be rapidly translated to the clinic [14, 16]. The design of the current silver contrast agent consisted of (a) a silver core for DE contrast, (b) a silica shell and (c) a polyethylene glycol coating to improve hydrophilicity and biocompatibility [26, 27]. The purpose of this study was to synthesize, characterize and test the performance of the prototype polyethylene glycol–silica–silver (PEG-SiO_2Ag) nanoparticle in mice. This

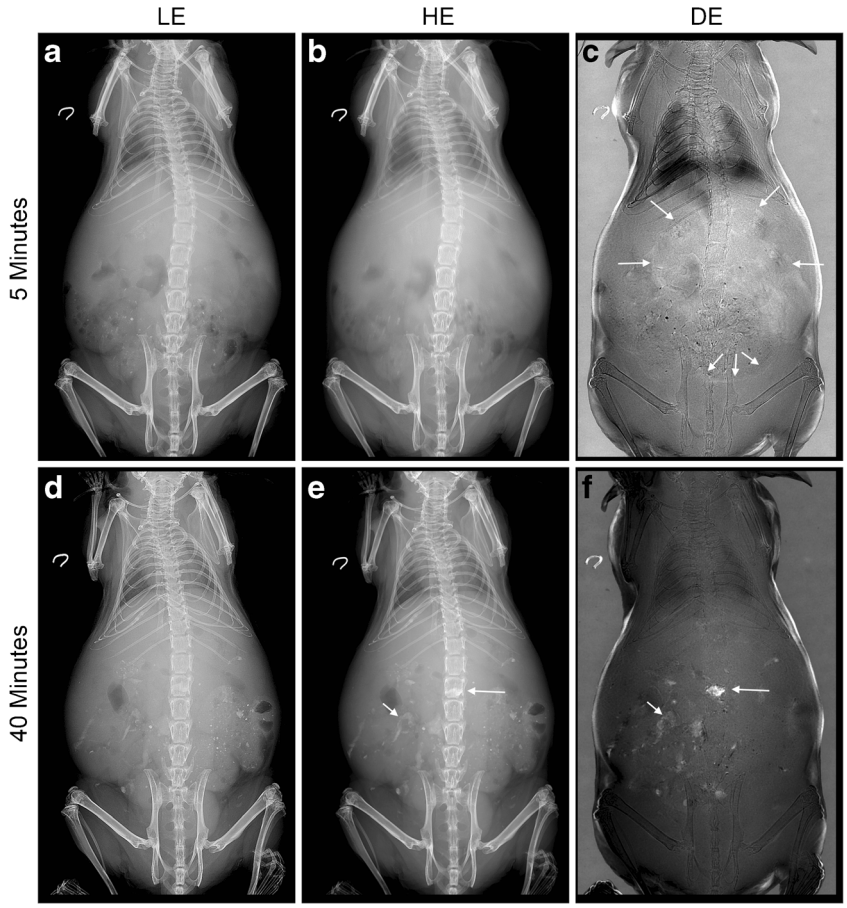

Fig. 4 LE, HE and DE images of a mouse immediately after administration of the silver contrast agent via intraperitoneal injection. The contrast from the silver (*arrows*) in the DE image highlights various organs. Concentration of the contrast agent in certain locations is seen over time

work is intended to serve as a point of reference for further improvements to the design of the nanoparticle as well as further testing of the existing design.

An important point to note regarding the design of the PEG-SiO_2Ag nanoparticle is the relatively large size of the silica shell compared to the rest of the nanoparticle. The dimensions of the nanoparticle imply that each particle consists of only 19 % silver by weight. The majority of an injected dose of PEG-SiO_2Ag nanoparticles therefore consists of silica, which is biocompatible. However, silica does not contribute to the primary function of DE contrast, indicating that in the future, the ratio of silica to silver can be optimized such that the silica shell is thinner compared with the diameter of the silver core. Hence, the percentage of the nanoparticle that is composed of the silver payload would be increased.

The short plasma half-life of the particles (Fig. 2a) is surprising given the design of the nanoparticle, and may point to a low degree of amination of the silica surface or attachment of the PEG ligand. The accumulation of the nanoparticles in the liver, spleen and lymph nodes (Fig. 2b) also suggests that the PEG coating in this formulation was insufficient in imparting substantial stealth characteristics to the nanoparticle, which

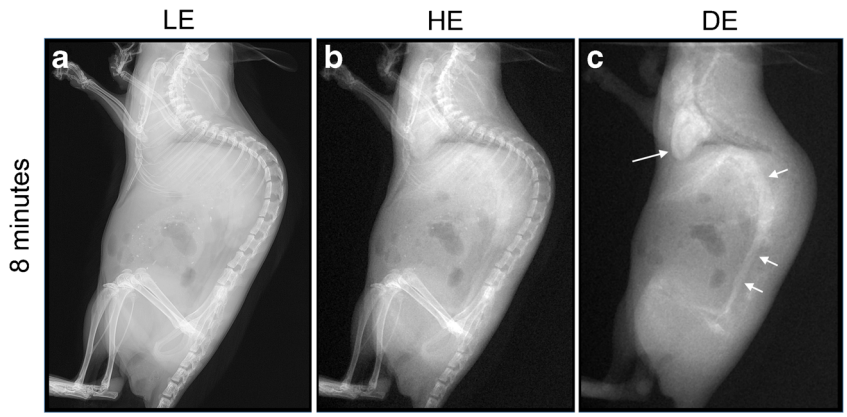

Fig. 5 LE, HE and DE images of a mouse after administration of silver nanoparticles via intravenous injection. The DE image successfully suppresses bone, soft tissue and air signals, while maintaining the vascular contrast. The heart (*long arrow*) and the abdominal aorta (*short arrow*) are clearly visualized, together with other smaller blood vessels in the abdomen and elsewhere

PEG typically provides [28]. These findings are consistent with previously published results, where it was found that the degree of PEGylation of a formulation has a strong influence on its biodistribution and pharmacokinetics [29, 30].

The PEG-SiO_2Ag nanoparticles were administered into mice via subcutaneous (Fig. 3a–c), intraperitoneal (Fig. 4) and intravenous (Fig. 5) injections and subsequently imaged using the previously developed DE method. In each case, the DE subtraction is able to suppress the anatomic signal variation while preserving the contrast from the silver nanoparticle agent. Conversely, contrast observed from the injection of gold nanoparticles in the single-energy images (Fig. 3g–i) was nullified in the DE image. As the K-edge of gold (80 keV) does not lie within the mammography energy range, the signal arising from the gold contrast agent cannot be separated from the underlying tissue using DE-weighted subtraction.

The animals injected with the PEG-SiO_2Ag nanoparticles were still alive 2 months after the injection, after which the mice were euthanized, indicating the biocompatibility of the agent. However, similar to the frequently used MRI contrast agent gadolinium [31], there is a safety concern with regards to silver ions [17, 32, 33]. Furthermore, the US Food and Drug Administration (FDA) will not approve a diagnostic agent that is not excreted well. Therefore, steps have to be taken to ensure adequate excretion. In this instance, the silica coating prevents silver ion leaching, but the large size of the nanoparticles prevents excretion [34, 35]. Hence design modifications to promote excretion are needed, such as the use of small, sub-5-nm nanoparticles that can be excreted via the kidneys or the use of silver chelates. We are currently actively working in this area by developing gold–silver alloy nanoparticles that have improved biocompatibility and are small enough for excretion.

In conclusion, silver nanoparticles can be used to increase the contrast of objects of interest in living systems using a dual-energy mammography imaging system. Further improvements in the design of the silver contrast agent to promote its biocompatibility and excretion may lead to the development of a contrast agent suitable for clinical translation.

Acknowledgments The scientific guarantor of this publication is Andrew Maidment. The authors of this manuscript declare relationships with the following companies: Unrelated to this project, one author (ADM) has received equipment grant support from Hologic, Inc. (Bedford, MA), is a member of the scientific advisory board of Gamma Medica, Inc. (Salem, NH) and Real-Time Tomography, LLC (Villanova, PA), and is a shareholder of Real-Time Tomography. This study has received funding by the Department of Defense (W81XWH-09-1-0055, W81XWH-11-1-0246) and National Institute of Health (R21-EB013754 and R03-CA171661). No complex statistical methods were necessary for this paper. Institutional review board approval was not required because patients were not used in the study. Approval from the institutional animal care committee was obtained.

Methodology: experimental, performed at one institution.

Compliance with ethical standards

Conflicts of Interest The authors are named as inventors on a patent pertaining to this work.

References

1. Wang AT, Vachon CM, Brandt KR, Ghosh K (2014) Breast density and breast cancer risk: a practical review. Mayo Clin Proc 89:548–557
2. Chen SC, Carton AK, Albert M, Conant EF, Schnall MD, Maidment ADA (2008) Initial clinical experience with contrast-enhanced digital breast tomosynthesis. Acad Radiol 14:229–238
3. Dromain C, Thibault F, Diekmann F et al (2012) Dual-energy contrast-enhanced digital mammography: initial clinical results of a multireader, multicase study. Breast Cancer Res 14:R94
4. Froeling V, Diekmann F, Renz DM et al (2013) Correlation of contrast agent kinetics between iodinated contrast-enhanced spectral tomosynthesis and gadolinium-enhanced MRI of breast lesions. Eur Radiol 23:1528–1536
5. Jochelson MS, Dershaw DD, Sung JS et al (2013) Bilateral contrast-enhanced dual-energy digital mammography: feasibility and comparison with conventional digital mammography and MR imaging in women with known breast carcinoma. Radiology 266: 743–751
6. Lewin JM, Isaacs PK, Vance V, Larke FJ (2003) Dual-energy contrast-enhanced digital subtraction mammography: feasibility. Radiology 229:261–268
7. Jochelson M (2014) Contrast-enhanced digital mammography. Radiol Clin N Am 52:609–616
8. Idee JM, Beaufils H, Bonnemain B (1994) Iodinated contrast media-induced nephropathy: pathophysiology, clinical aspects and prevention. Fundam Clin Pharmacol 8:193–206
9. Stacul F, van der Molen AJ, Reimer P et al (2011) Contrast induced nephropathy: updated ESUR Contrast Media Safety Committee guidelines. Eur Radiol 21:2527–2541
10. Pan D, Roessl E, Schlomka JP et al (2010) Computed tomography in color: Nanok-enhanced spectral CT molecular imaging. Angew Chem 49:9635–9639
11. Pan D, Schirra CO, Senpan A et al (2012) An early investigation of ytterbium nanocolloids for selective and quantitative "multicolor" spectral CT imaging. ACS Nano 6:3364–3370
12. Allijn IE, Leong W, Tang J et al (2013) Gold nanocrystal labeling allows low density lipoprotein imaging from the subcellular to macroscopic level. ACS Nano 7:9761–9770
13. Cormode DP, Roessl E, Thran A et al (2010) Atherosclerotic plaque composition: analysis with multicolor CT and targeted gold nanoparticles. Radiology 256:774–782
14. Karunamuni R, Tsourkas A, Maidment ADA (2014) Exploring silver as a contrast agent for contrast-enhanced dual-energy x-ray breast imaging. Br J Radiol 87:20140081
15. Karunamuni R, Zaki AA, Popov AV et al (2012) An examination of silver as a radiographic contrast agent in dual-energy breast x-ray imaging. LNCS - IWDM 7361:418–425
16. Karunamuni R, Maidment ADA (2014) Search for novel contrast materials in dual-energy x-ray breast imaging using theoretical modeling of contrast-to-noise ratio. Phys Med Biol 59:4311–4324
17. Liu J, Hurt RH (2010) Ion release kinetics and particle persistence in aqueous nano-silver colloids. Environ Sci Technol 44: 2169–2175

18. Torchilin VP (2007) Micellar nanocarriers: pharmaceutical perspectives. Pharm Res 24:1–16
19. Silvert P-Y, Duvauchelle N, Vijayakrishnan V, Elhsissen KT (1996) Preparation of colloidal silver dispersions by the polyol process. J Mater Chem 6:573–577
20. Graf C, Vossen DLJ, Imhof A, van Blaaderen A (2003) A general method to coat colloidal particles with silica. Langmuir 19: 6693–6700
21. Blasi F, Oliveira BL, Rietz TA et al (2015) Radiation dosimetry of the fibrin-binding probe 64Cu-FBP8 and its feasibility for PET imaging of deep vein thrombosis and pulmonary embolism in rats. J Nucl Med 56:1088–1093
22. Cai QY, Kim SH, Choi KS et al (2007) Colloidal gold nanoparticles as a blood-pool contrast agent for x-ray computed tomography in mice. Investig Radiol 42:797–806
23. Naha PC, Chhour P, Cormode DP (2015) Systematic in vitro toxicological screening of gold nanoparticles designed for nanomedicine applications. Toxicol In Vitro 29:1445–1453
24. Lau KC, Roth S, Maidment ADA (2014) 2D and 3D registration methods for dual-energy contrast-enhanced digital breast tomosynthesis. Proc SPIE 9033, Medical Imaging 2014: Physics of Medical Imaging:90335W
25. Gang GJ, Varon CA, Kashani H et al (2009) Multiscale deformable registration for dual-energy x-ray imaging. Med Phys 36:351–363
26. van Schooneveld MM, Vucic E, Koole R et al (2008) Improved biocompatibility and pharmacokinetics of silica nanoparticles by means of a lipid coating: a multimodality investigation. Nano Lett 8:2517–2525
27. Koole R, van Schooneveld MM, Hilhorst J et al (2008) Paramagnetic lipid-coated silica nanoparticles with a fluorescent quantum dot core: a new contrast agent platform for multimodality imaging. Bioconjug Chem 19:2471–2479
28. Torchilin VP (2002) PEG-based micelles as carriers of contrast agents for different imaging modalities. Adv Drug Deliv Rev 54: 235–252
29. Klibanov AL, Maruyama K, Beckerleg AM, Torchilin VP, Huang L (1991) Activity of amphipathic poly(ethylene glycol)-5000 to prolong the circulation time of liposomes depends on the liposome size and is unfavorable for immunoliposome binding to target. Biochim Biophys Acta 1062:142–148
30. Cormode DP, Skajaa GO, Delshad A et al (2011) A versatile and tunable coating strategy allows control of nanocrystal delivery to cell types in the liver. Bioconjug Chem 22:353–361
31. Todd DJ, Kay J (2008) Nephrogenic systemic fibrosis: an epidemic of gadolinium toxicity. Curr Rheumatol Rep 10:195–204
32. Hussain SM, Hess KL, Gearhart JM, Geiss KT, Schlager JJ (2005) In vitro toxicity of nanoparticles in BRL 3A rat liver cells. Toxicol In Vitro 19:975–983
33. Samberg ME, Oldenburg SJ, Monteiro-Riviere NA (2010) Evaluation of silver nanoparticle toxicity in skin in vivo and keratinocytes in vitro. Environ Health Perspect 118:407–413
34. Choi HS, Liu W, Misra P et al (2007) Renal clearance of quantum dots. Nat Biotechnol 25:1165–1170
35. Fitzpatrick JAJ, Andreko SK, Ernst LA, Waggoner AS, Ballou B, Bruchez MP (2009) Long-term persistence and spectral blue shifting of quantum dots in vivo. Nano Lett 9:2736–2741